Christine L. de Lancea
UC High Performance Computing,
University of Canterbury,
Christchurch, Canterbury 8041, New Zealand
e-mail: christine.l.french@hotmail.com

Tim David
Professor
Mem. ASME
UC High Performance Computing,
University of Canterbury,
Christchurch, Canterbury 8041, New Zealand
e-mail: tim.david@canterbury.ac.nz

Jordi Alastruey
Department of Biomedical Engineering,
Division of Imaging Sciences
and Biomedical Engineering,
King's College London,
King's Health Partners,
St. Thomas' Hospital,
London SE1 7EH, United Kingdom
e-mail: jordi.alastruey-arimon@kcl.ac.uk

Richard G. Brown
Institute of Fundamental Sciences,
Massey University,
Palmerston North, Manawatu-Wanganui 4474,
New Zealand
e-mail: r.g.brown@massey.ac.nz

Recruitment Pattern in a Complete Cerebral Arterial Circle

Blood flow through a vessel depends upon compliance and resistance. Resistance changes dynamically due to vasoconstriction and vasodilation as a result of metabolic activity, thus allowing for more or less flow to a particular area. The structure responsible for directing blood to the different areas of the brain and supplying the increase flow is the cerebral arterial circle (CAC). A series of 1D equations were utilized to model propagating flow and pressure waves from the left ventricle of the heart to the CAC. The focus of the current research was to understand the collateral capability of the circle. This was done by decreasing the peripheral resistance in each of the efferent arteries, up to 10% both unilaterally and bilaterally. The collateral patterns were then analyzed. After the initial 60 simulations, it became apparent that flow could increase beyond the scope of a 10% reduction and still be within in vivo conditions. Simulations with higher percentage decreases were performed such that the same amount of flow increase would be induced through each of the efferent arteries separately, same flow tests (SFTs), as well as those that were found to allow for the maximum flow increase through the stimulated artery, maximum flow tests (MFTs). The collateral pattern depended upon which efferent artery was stimulation and if the stimulation was unilaterally or bilaterally induced. With the same amount of flow increase through each of the efferent arteries, the MCAs (middle cerebral arteries) had the largest impact on the collateral capability of the circle, both unilaterally and bilaterally. [DOI: 10.1115/1.4031469]

Keywords: complete cerebral arterial circle, resistance, collateral patterns, efferent arteries

1 Introduction

Protected by the bones of the skull is the most important organ of the human body. Even though it weighs only 2% of the total body weight, the brain receives nearly 20% of the cardiac output. This precious organ is divided into four lobes which are responsible for interpreting different stimuli. When this activation occurs, local metabolism increases. The brain needs to redirect blood to these areas to replace the diminished resources and dispose of the waste products. It must do this without depleting the blood source from other areas which could cause loss of consciousness, permanent brain damage, or even death. The structure responsible for this recruitment and redistribution of blood is called the CAC.

The CAC (more commonly referred to as the circle of Willis) is responsible for allotting the inflow of blood from the basilar artery (BA) and internal carotid arteries (ICAs) to the anterior, middle, and posterior cerebral arteries to adequately profuse the brain. Due to various reasons, plaque can build up in one of the main feeding arteries causing occlusion or blockage of blood. In order for surgeons to preform an endarterectomy, removal of the plaque, the feeding artery has to be clamped shut. This procedure could be life saving but roughly 10–20% of patients possess CAC configurations that make them more susceptible to cerebral ischemia if one of the carotids were to be clamped, stenosed, or occluded [1]. Therefore, it is of the utmost importance for surgeons to investigate the circle before preforming this or any other operation that require the clamping of cerebral arteries. However, the collateral ability of the CAC is not just for cases of stenosis, occlusion, or surgery.

The CAC is used to distribute blood to brain tissue so as to supply local metabolic demands. Blood flow is influenced by the resistance and compliance of the distal vessels perfusing the cortical tissue. According to Poiseuille's law, resistance, R, is inversely proportional to the fourth power of radius which varies according to metabolic demands

$$R = \frac{8\eta L}{\pi r^4} \tag{1}$$

where r is the radius, η is the blood viscosity, and L is the length. Taking the derivative of Eq. (1) with respect to radius, ($|\delta R| = (32\eta L/\pi r^5)\delta r$) demonstrates how a small change in radius has a large impact on the resistance and, therefore, the flow. Using the right anterior cerebral artery (ACA) as an example, decreasing the radius by 1% will increase the resistance by roughly 5%.

Local metabolism, with a subsequent increase in neuronal activity, requires larger amounts of oxygen and glucose to be transported to the activated site. This is achieved by increasing the radius of the local perfusing arterioles, a mechanism termed neurovascular coupling [2–6], consequently changing the peripheral resistance (Eq. (1)). It is not fully understood how sensitive cerebral flow is to these changes. A one-dimensional computer model is utilized in this study as they have low computational cost and allow for the fuller development of the flow wave profile, such that when a wave propagates through the arterial tree, at each bifurcation encountered part of the wave is reflected and combines with the subsequent forward traveling waves to produce a full profile. An example of this is the dicrotic notch which is a combination of the closure of the aortic valve and the reflected waves [7].

The current model is used to study the effects of decreasing peripheral resistance on blood flow through the circle. While most papers focus on blood flow through the efferent arteries in the event of stenosis or occlusion [8–14], just to list a few, as a means to show the collateral capability of the CAC, the current

Manuscript received March 19, 2015; final manuscript received August 24, 2015; published online September 18, 2015. Assoc. Editor: Alison Marsden.

simulations show the use of collateral vessels within the circle whilst not under such stress, particularly in regard to the communicating arteries. The goal of this research is to comprehend the correlation between resistance of the cortical vascular bed (termed peripheral resistance) and the collateral pattern of blood flow through a complete CAC for stimulations that would occur within a nonstressed environment. This study is also used to fill a void that is present within the literature as a reference for future projects.

2 Methods and Material

The 1D computer model utilized was developed by the Department of Aeronautics, Imperial College and the Faculty of Medicine, Division of Imaging Sciences and Biomedical Engineering, King's College London, King's Health Partners, St. Thomas, Hospital, London [15]. It solves nonlinear 1D equations for compliant vessels under the influence of established initial and boundary conditions. The model has been validated against 3D model numerical results [16] and in vitro data [17]. Sections 2.1 and 2.2 describe the properties of the model and are based on the work presented in Refs. [8], [18], and [19].

2.1 Mesh Definition and Governing Equations. Each artery is defined as a domain. The model divides the domains into segments that are connected by nodes. Every domain contains the number of segments, the quadrature order of the segment, and the upper and lower spatial coordinates. The domains are compliant tubes whose properties are describable at x, a single axial location. The flow is laminar and is evaluated by the long wavelength approximation due to the pulse wavelengths being 3 orders of magnitude larger than the diameter of the vessels and 1 order of magnitude larger than the longest vessel segment.

The model simulates incompressible, Newtonian fluid employing equations for conservation of mass and momentum, respectively

$$\frac{\partial A}{\partial t} + \frac{\partial (AU)}{\partial x} = 0 \tag{2}$$

$$\frac{\partial U}{\partial t} + U\frac{\partial U}{\partial x} = -\frac{1}{\rho}\frac{\partial p}{\partial x} + \frac{f}{\rho A} \tag{3}$$

where x is the axial coordinate; t is time; $A(x,t)$ is the cross-sectional area of the artery; $U(x,t)$ is the average axial velocity; $p(x,t)$ is the average internal pressure over the cross-sectional area; ρ is the density of blood, 1050 kg/m^3; and $f(x,t)$ is the friction force per unit of length. This is represented by the equation

$$f = -22\pi\mu U \tag{4}$$

where μ is the viscosity of blood, 4.5 mPa s.

To close the system, an equation is needed to define the pressure–area relationship which is assumed to be

$$p = p_0 + \frac{\beta}{A_0}\left(\sqrt{A} - \sqrt{A_0}\right) \tag{5}$$

$$\beta = \frac{\sqrt{\pi}hE}{(1-\sigma^2)} \tag{6}$$

where h and A_0 are the wall thickness and sectional area at the reference state of (p_0, U_0), these are assumed to be zero. E is the Young's Modulus, a measure of arterial stiffness represented as stress over strain. The Poisson ratio, σ, is the negative ratio of transverse strain divided by axial strain. For biological tissues, this is set equal to 1/2. β is a constant parameter of arterial stiffness related to the speed of the pulsatile waves generated by the beating heart, c, which is expressed as

$$c^2 = \frac{\beta}{2\rho A_0}\sqrt{A} \tag{7}$$

The PDEs (partial differential equations, Eqs. (2), (3), (5), and (6)) within each domain were solved by a second-order Adams–Bashforth time–space integration scheme and discontinuous Galerkin with spectral/*hp* spatial discretization with a polynomial order, $P = 8$. A high P and small timestep allowed for a fast phase convergence. These methods were also chosen as they possess the ability to analyze propagating waves of different frequencies without excessive diffusion and dispersion errors.

2.2 Boundary Conditions and Bifurcations. The arterial circulation is a highly complicated system. Leading computer scientists and math modelers helped to simplify models to ease computational demands. In order to do this, many vascular simulations truncate vessels after a determined number of bifurcations and couple the ends to lumped models. The characteristics of the vessels that would naturally exist beyond the terminated point are summed up and used as the terminal parameters. In order to replicate a flow wave profile in response to these truncations, accurate values for peripheral resistance and compliance are necessary.

Compliance is the elasticity of a vessel that stores energy from systolic periods, when the heart contracts, to balance pressure in the vascular system during diastolic periods, when the heart relaxes. Vessels become more rigid or less compliant the older a person gets but does not change dramatically over a short period of time. Therefore, compliance is kept as a constant in the simulations and the peripheral resistance is changed. This decision is supported as the wave profiles do not deform when compliance is kept static (see Fig. 1).

In each artery, the hyperbolic system of PDEs (Eqs. (2), (3), (5), and (6)) was solved using the following boundary conditions. At the inlet of the ascending aorta, the periodic inflow rate, $Q(t)$, was set to a period of 1 s. Each period had half of a sinusoidal wave with a peak of $\hat{Q}$, 485 ml/s, for a duration of 0.3 s, τ. This represented the systolic period of the cardiac cycle with a flowrate equal to zero in the resting phase, diastole

$$Q(t) = \begin{cases} \hat{Q}\sin\left(\dfrac{\pi t}{\tau}\right) & \text{if } t < \tau \\ 0 & \text{otherwise} \end{cases} \tag{8}$$

When the flowrate equals zero, the boundary condition behaves as a total reflection, mimicking the closure of the aorta valve.

Within the junction nodes of the model between the different domains, continuity of total pressure and conservation of mass are enforced by implementing: $p + (1/2)\rho U^2$, which is held as a constant. At the terminal vessels, a three-element Windkessel model—characteristic impedance (R_1), compliance (C), peripheral resistance (R_2)—partially reflects and smooths incoming waves which is more physiologically correct than a complete reflection. The equation for balancing the pressure differences is

$$p_{1D} + CR_2\frac{dp_{1D}}{dt} = p_v + (R_1 + R_2)Q_{1D} + R_1CR_2\frac{dQ_{1D}}{dt} \tag{9}$$

where Q_{1D} is the volume flowrate, p_{1D} is the pressure at the terminal end of the artery, and p_v is the pressure at the entrance of the venous system, set to 5 mmHg; illustrated in Fig. 2. Total arterial compliance is the sum of the elasticity of the arteries after the point of truncation. Peripheral resistance, which can be calculated using Poiseuille's equation (Eq. (1)), is the sum of all the resistance of the arteries that have been excluded from the numerical discretization.

The values for the systemic arteries were taken from the study of Ref. [20], who regarded parameters found in the literature taken during surgery. Length and radius of the arteries composing the CAC were taken from Refs. [21] and [22]. Measurements for Ref. [21] were derived from the literature using X-ray projection imaging, synthetic resin, CT imaging, and cadaveric measurements, while Ref. [22] used MRA scans and available literature. Refer to Table 1 for the list of values and abbreviation descriptions.

2.3 Variations in Peripheral Resistance. Poiseuille's equation indicates that changes in radius have the greatest impact on peripheral resistance. This is the result of changing local metabolic needs. When a person is introduced to a stimulus, specific areas of the brain become more active. For example, when one opens their eyes after being closed the occipital lobe, which perceives visual stimuli, begins to interpret the surroundings by using a series of chemical pathways. This activation requires more blood to replenish the local resources and dispense of the waste products by inducing vasodilation. This dilating of the vessels decreases the local resistance and allows for more blood flow to the area.

To test the direct affect of decreasing R_2 on flow, a model consisting of the major arteries leaving the heart that feed into the CAC and its main efferent arteries was compiled (Fig. 3). Once base values were established, they were used to compare against an incrementally decreasing R_2; 1%, until a decrease of 10% was reached. A 10% decrease was chosen as it would give a good representation of the development of the collateral patterns. The results of these 60 simulations demonstrated the effectiveness of the collateral pathways of the CAC.

A literature review was then conducted to find the average change in flow as a result of local stimulation to establish physiological boundaries for the simulations. However, most studies focused on velocity increases due to exercise, arithmetic, or visual stimulation [6,23–27], but not on flow directly from decreasing resistance. These values were derived by electrocardiogram, photoplethysmography, and transcranial Doppler sonography. The current model was used to calculate similar velocity averages, to allow for comparison with the literature, which in turn was used to determine the correlated flow values.

A study by Kelley et al. [23] observed blood velocity changes in the ACAs, MCAs, and PCAs (posterior cerebral arteries) due to stimulation of either playing video games or performing arithmetic. Percentages were calculated from the values given in the paper. The highest percentage of velocity increase reported for one ACA was 5.8%. To achieve the desired velocity increase, an R_2 reduction of 7% was needed. The largest change for one MCA was reported at 11.9% and 15.8% for one PCA. Both the MCA and PCA decreases surpassed the scope of a 10% R_2 decrease.

Regarding the bilateral tests, the ACAs were reported to have a 3.9% increase in velocity [23] which best correlated with an R_2 reduction of 5%. The MCAs and the PCAs exceeded the results for a bilateral 10% decrease. The velocity in the MCA is being recorded in their study at an increase of 9.0%. The PCAs were reported with an increase of 15.8%.

When comparing the work of Kelley et al. [23] with the current study, results showed that the peripheral resistance can decrease more than 10%. The next step was to find the largest percentage differences for velocity changes available in the literature for each pair of efferent arteries to find the correlating flow. Over 120 simulations were performed to find the R_2 values that would yield the desired velocity increases and all the percentage decreases in between.

The highest velocity changes for the ACAs were 25.0% unilaterally and 23.0% bilaterally [24]. To obtain the value closest to the desired unilateral test, the R_2 was decreased by 24%. For the bilateral test, the R_2 was also decreased by 24%. The MCAs were reported with an increase of 21.0% unilaterally and 18.0% bilaterally [24]. These were obtained by a unilateral resistance reduction of 21% and 19% bilaterally. The PCAs had a unilateral increase of 31.0% [27] and 28.0% bilaterally [6]. A decrease of 29% unilaterally and a bilateral decrease of 28% yielded the desired velocity changes.

Once resistance values had been established, they were used to determine the corresponding flow. The unilateral ACA test resulted in a 24.2% increase. For the bilateral simulations, the flow increased by 23.3%. The unilateral MCA test resulted in a 21.0% flow increase. The bilateral test yielded a 17.9% rise in flow. The unilateral PCA had a correlated 30.3% flow increase. In the bilateral simulations, the flow reflected a 27.6% increase. These tests were collectively referred to as the MFTs. A summary of these values can be found in Table 2.

Even though both of the MCA tests had the smallest decrease in R_2, they exhibited the largest increase in flow. Unilaterally, the

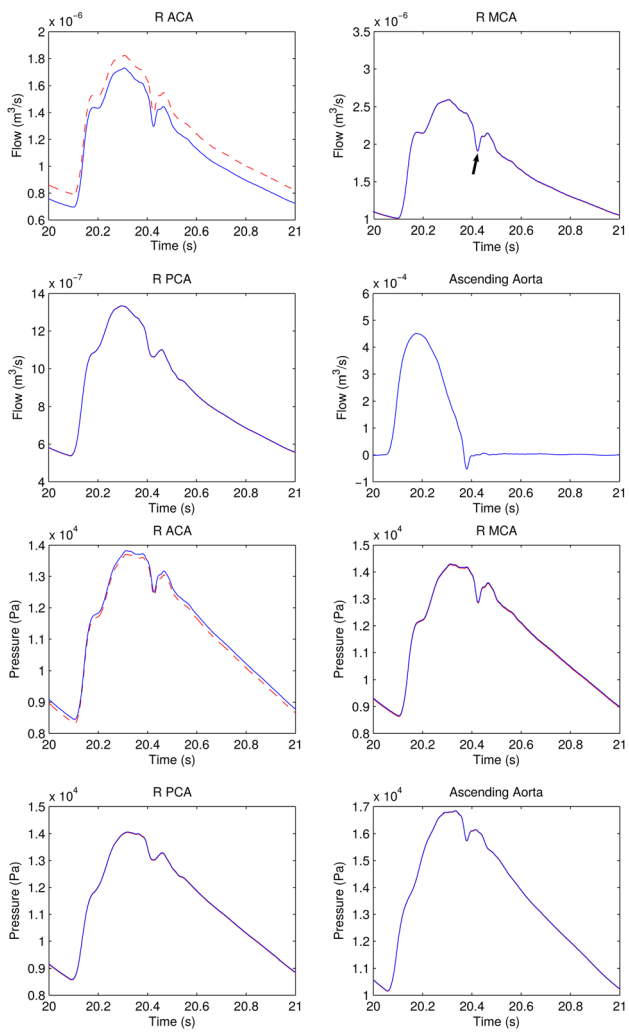

Fig. 1 Demonstrates an example of the flow (top four figures) and pressure (bottom four) wave profiles. These are from a unilateral R_2 decrease of 10% in the right ACA shown by dashed line against the control with no reductions, solid line. A dicrotic notch indicated by arrow.

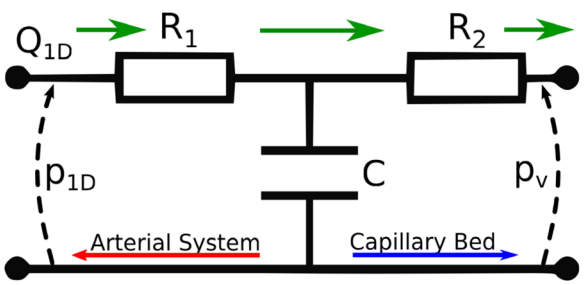

Fig. 2 A three-element Windkessel utilized in Eq. (9), where the pressure at the terminal end of an artery—p_{1D}—is used to match that of the pressure of the truncated vessels. Q_{1D}—volumetric flow, p_v—venous pressure, R_1—characteristic impedance, C—compliance, R_2—peripheral resistance, top arrows—flow.

flow increased by 0.36 cm^3/s and by a total of 0.62 cm^3/s in the bilateral simulation. The smallest increase in flow was found in the PCAs for both unilateral and bilateral tests, with an increase of 0.27 cm^3/s and 0.49 cm^3/s, respectively. These latter values were used to observe how the CAC compensated in the event that the same amount of flow increase was introduced into the ACAs, MCAs, and PCAs individually. The resulting tests were collectively known as the SFTs. The subsequent values given were based on an average of 10 cardiac cycles.

3 Results

The R_2 was decreased from 1% to 10% for the ACAs, MCAs, and PCAs; both unilaterally, arbitrarily on the right, and bilaterally. For simplicity reasons, the pairs of efferent arteries were considered independently from each other. Changes in flow were considered notable if it was over 1%, except in the cases of the ACoA (anterior communicating arteries) and PCoAs (posterior communicating arteries). If the flow in these latter vessels were not of the same magnitude as the neighboring efferent arteries, the flow was not considered notable. This is because flow through these vessels is very small. Some papers within the literature state that flow through the communicating arteries of a complete circle is negligible [28–34]. Percentages for the communicating arteries were not presented in the figures as the flow increase were sometimes over 1000% but their roles as collateral pathways were discussed where appropriate. While the paired arteries were symmetrical in dimensions on either side of the circle, flow through them was not identical even at the baseline values or in bilateral stimulations. This is attributed to the differences in the paths of blood flow from the heart to the corresponding sides. Similar asymmetries can also be found within the literature [6,23–25].

In each case where R_2 was decreased by 1%, there was no notable change in flow detected in any of the vessels. With a decrease of 10%, flow change in the unaltered efferent arteries remained less than 1%, regardless if it was a unilateral or bilateral reduction. This was the case for all 1–10% reductions in the ACAs, MCAs, and PCAs.

Flow within the right ACA increased by 8.9% after a 10% reduction of the R_2. The right and left ACA A1s (proximal segment of the anterior cerebral arteries) were the primary pathways used to meet the increasing flow demands. These were followed by the ICAs and ICA IIs (segment of the internal carotid arteries that lay within the cerebral arterial circle) (Fig. 4). The posterior portion of the circle was not exploited to restore balance.

When the peripheral resistance of the ACAs was reduced bilaterally, the recruitment pattern of the vessels differed from those with unilateral reduction (Fig. 5). With an R_2 decrease of 10%, each ACA exhibited a flow increase of 8.5%. Though the recruitment pattern differed from the unilateral tests, the compensatory arteries remained the same. The ACA A1 segments were the primary collateral vessels followed by the ICAs and the ICA IIs.

Table 1 Parameters for the systemic arteries was originally taken from Ref. [20]. Values for the lengths of the vessels that comprise the CAC was taken from Ref. [21] and the radii from Ref. [22], as presented in Ref. [8] whose thickness and elastic modulus values were also used. L—left, R—right, ACA—anterior cerebral artery, ACA A1—proximal segment of the ACA, ACoA—anterior communicating artery, BA—basilar artery, CCA—common carotid artery, ECA—external carotid artery, ICA—internal carotid artery, ICA II—segment of the ICA that lays within the CAC, MCA—middle cerebral artery, PCA—posterior cerebral artery, PCA P1—proximal segment of the PCA, PCoA—posterior communicating artery, VA—vertebral artery.

Original values used in the 1D model for the vessels that lead from the heart to the CAC

Arterial segment		Length (cm)	Initial radius (cm)	Thickness (cm)	Elastic modulus (10^6 Pa)	Peripheral resistance (10^9 Pa s m^{-3})	Peripheral compliance (10^{-10} m^3 Pa^{-1})
1	Ascending aorta	4.0	1.200	0.163	0.4	—	—
2	Aortic arch I	2.0	1.120	0.126	0.4	—	—
3	Brachiocephalic	3.4	0.620	0.080	0.4	—	—
4	Aortic arch II	3.9	1.070	0.115	0.4	—	—
5	L. CCA	20.8	0.250	0.063	0.4	—	—
6	R. CCA	17.7	0.250	0.063	0.4	—	—
7	R. subclavian	3.4	0.423	0.067	0.4	—	—
8	Thoracic aorta	15.6	0.999	0.110	0.4	0.18	38.70
9	L. subclavian	3.4	0.423	0.067	0.4	—	—
10	L. ECA	17.7	0.150	0.038	0.8	5.43	1.27
11	L. ICA	17.7	0.200	0.050	0.8	—	—
12	R. ICA	17.7	0.200	0.050	0.8	—	—
13	R. ECA	17.7	0.150	0.038	0.8	5.43	1.27
14	R. VA	14.8	0.136	0.034	0.8	—	—
15	R. brachial	42.2	0.403	0.067	0.4	2.68	2.58
16	L. brachial	42.2	0.403	0.067	0.4	2.68	2.58
17	L. VA	14.8	0.136	0.034	0.8	—	—
18	L. ICA II	0.5	0.200	0.050	1.6	—	—
19	L. PCoA	1.5	0.073	0.018	1.6	—	—
20	R. PCoA	1.5	0.073	0.018	1.6	—	—
21	R. ICA II	0.5	0.200	0.050	1.6	—	—
22	BA	2.9	0.162	0.040	1.6	—	—
23	L. MCA	11.9	0.143	0.036	1.6	5.97	1.16
24	R. MCA	11.9	0.143	0.036	1.6	5.97	1.16
25	L. ACA A1	1.2	0.117	0.029	1.6	—	—
26	R. ACA A1	1.2	0.117	0.029	1.6	—	—
27	L. PCA P1	0.5	0.107	0.027	1.6	—	—
28	R. PCA P1	0.5	0.107	0.027	1.6	—	—
29	L. ACA	10.3	0.120	0.030	1.6	8.48	0.82
30	R. ACA	10.3	0.120	0.030	1.6	8.48	0.82
31	ACoA	0.3	0.074	0.019	1.6	—	—
32	L. PCA	8.6	0.105	0.026	1.6	11.08	0.62
33	R. PCA	8.6	0.105	0.026	1.6	11.08	0.62

A maximum reduction of R_2 in the right MCA yielded a flow increase of 9%. The main collateral arteries were the ipsilateral ACA A1 and ICA II segments followed closely by their left counterparts. However, in this case the right ACA A1 expressed a notable flow decrease to compensate for the demand. While the anterior portion of the CAC was the primary source to maintain flow balance, the right PCA P1 (proximal segment of the posterior cerebral artery) segment was utilized at an R_2 decrease of 7% and higher (Fig. 6).

When the peripheral resistance was decreased bilaterally in the MCAs, the posterior portion of the circle becomes an important route to supplement blood flow (Fig. 7). To compensate for an increase of 8.7% in both efferent arteries, the ICAs and ICA IIs became the main collateral pathways. The BA and the PCA P1 segments were also recruited for compensation at an R_2 decrease of 7% and higher.

An R_2 reduction of 10% in the right PCA was compensated by the vessels of the posterior CAC. The primary pathway was the right PCA P1 followed by the BA then left PCA P1. Here, the left PCA P1 exhibited a notable reduction in flow (Fig. 8). A maximum decrease bilaterally in the PCAs utilized the same vessels. However, when both efferent arteries were stimulated, all three arteries were utilized equally (Fig. 9).

When first reviewing the results, the collateral ability of the CAC is very apparent. Even with a bilateral reduction of the R_2 up to 10% in the largest pair of efferent arteries, the MCAs, there is no notable flow change within the remaining two pairs. This shows that a complete CAC does use the collateral pathways during stimulation of regions of the brain without the presence of a stenosed or occluded artery. More importantly, it shows the ability of the circle to recruit blood to supply the increase in demand without depleting blood flow to the other areas of the brain.

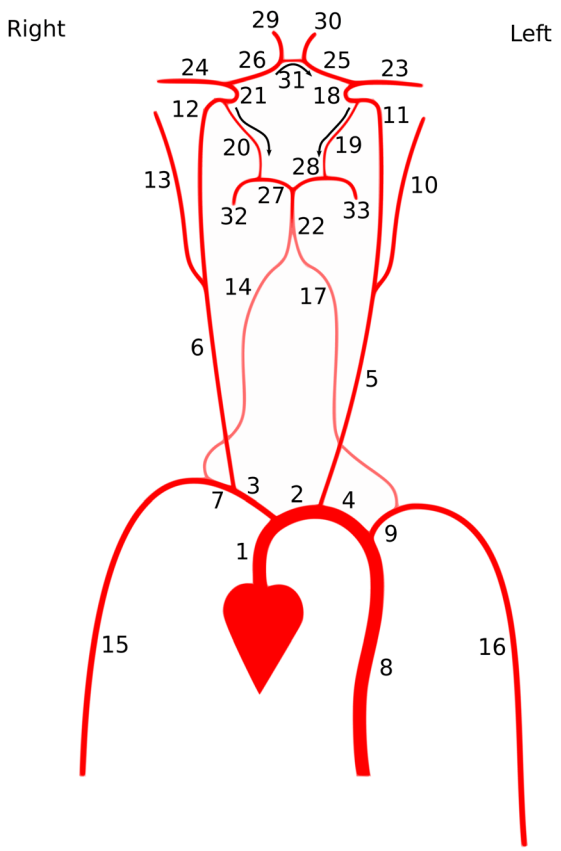

Fig. 3 Depicts the vessels used in the simulations. Numbers correlate with Table 1. Arrows indicate positive flow in the communicating arteries. Based on the work by Alastruey et al. [8].

Decreasing the peripheral resistance of the individual efferent arteries, up to 10% both unilaterally and bilaterally, did not have a notable effect on the remaining efferent arteries. This attests to the collateral ability of the CAC and how it recruits blood from the afferent arteries to distribute it through the communicating and connecting vessels compensating for an increase in metabolic demand. Connecting arteries are considered to be the vessels within the circle that are not the communicating arteries: ACA A1s, ICA IIs, and PCA P1s. Depending on which efferent artery is stimulated and if the stimuli is unilateral or bilateral, different vessel recruitment patterns are observed in order to maintain homeostasis.

4 Discussion

4.1 Comparing the Connecting Arteries. Flow between the two ACA A1 segments appeared to be highly correlated and the most important collateral pathway in regard to both unilateral and bilateral reductions of the ACAs and unilateral decrease of the MCAs. When the right ACA A1 exhibited notable flow change, so did the left either at the same percentage of R_2 decrease or at the next reduction. This correlation is most likely due to the short connection they share, the ACoA. Decreasing the peripheral resistance of the right MCA induces a flow reduction in the right ACA A1 and increase in the left, pulling the blood from the contralateral side through the ACA A1s and ACoA.

The pattern of recruitment for the ACA A1, in regard to reduction of the ACAs, was expected as blood has to flow through the proximal segments to reach the distal portions. Flow in the ACoA was considered negligible under the conditions stated previously. However, it still contributed largely to the maintenance of homeostasis in the event of unilateral reduction of the ACAs. Flow in the ACoA was considered positive if movement was from right to left. At a unilateral ACA reduction of 10%, there was a decrease of 85.7% in blood flow within the ACoA. Flow reduced from 0.045 cm^3/s to 0.007 cm^3/s, a difference of 0.038 cm^3/s. This indicated that smaller amounts of blood were being routed to the left side of the CAC from the right. This reflected the changes in the left ACA A1 which had an increase from 1.107 cm^3/s to 1.143 cm^3/s, a difference of 0.036 cm^3/s. The compensated flow from the left ACA A1 and ACoA brought a balance to the flow of the circle with only a 0.3% decrease in the flow of the left ACA.

Unilateral reduction of the MCAs showed that blood was recruited from the right ACA A1 reducing the amount of flow it would contribute to the ipsilateral ACA. The ACoA was used to restore the balance. At a decrease of 10% in the right MCA, the ipsilateral ACA A1 was decreased by 0.044 cm^3/s, the ACoA had a reduction in flow of 0.037 cm^3/s, and the contralateral ACA A1 had an increase of 0.034 cm^3/s. Showing the blood being redistributed from the left ACA A1 through the ACoA to meet the demand, attesting to the collateral capability of the CAC.

Studying the recruitment flow pattern reveals that a unilateral reduction of the MCAs has a greater impact on the CAC system

Table 2 The percentage of R_2 reduction needed to achieve the maximum flow increase in each artery. Values for the bilateral results were a sum of the paired activated vessels.

		Flow increase	
Stimulated artery	R_2 reduction (%)	(%)	(cm^3/s)
Unilateral, MFT			
ACA	24	24.2	0.28
MCA	21	21.0	0.36
PCA	29	30.3	0.27
Bilateral, MFT			
ACAs	24	23.3	0.54
MCAs	19	17.9	0.62
PCAs	28	27.6	0.49

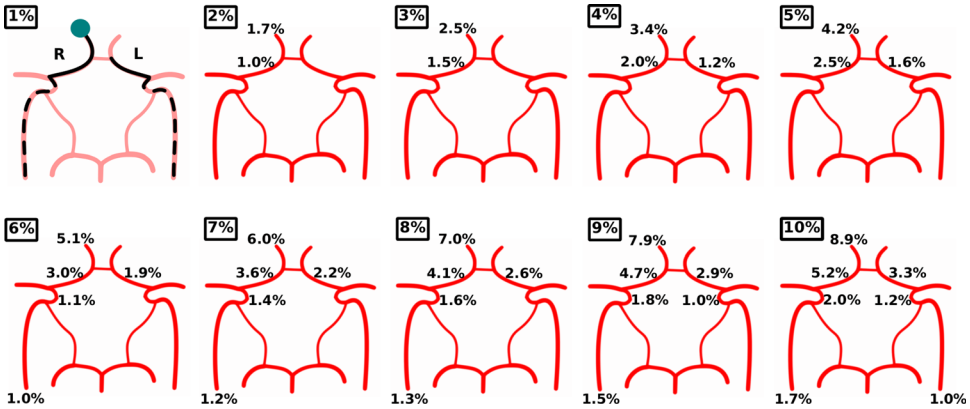

Fig. 4 Percentages of flow increase are shown at each decrease of the peripheral resistance values, indicated by the percentage in the boxes. Since a 1% did not yield notable flow, the schematic was used to denote the vessel with the decreasing R_2, highlighted by the circle, and collateral pathways. R—right, L—left, solid line—vessels that express notable flow change with a R_2 decrease of up to 5%, rounded dashed line up to a 10% decrease.

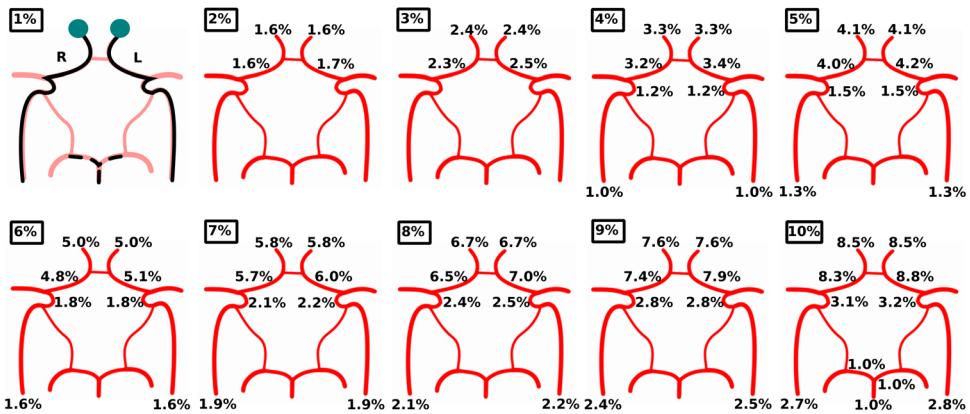

Fig. 5 Percentages of flow increase are shown at each decrease of the peripheral resistance values, indicated by the percentage in the boxes. Since a 1% did not yield notable flow, the schematic was used to denote the vessels with the decreasing R_2, highlighted by the circles, and collateral pathways. R—right, L—left, solid line—vessels that express notable flow change with a R_2 decrease of up to 5%, rounded dashed line up to a 10% decrease.

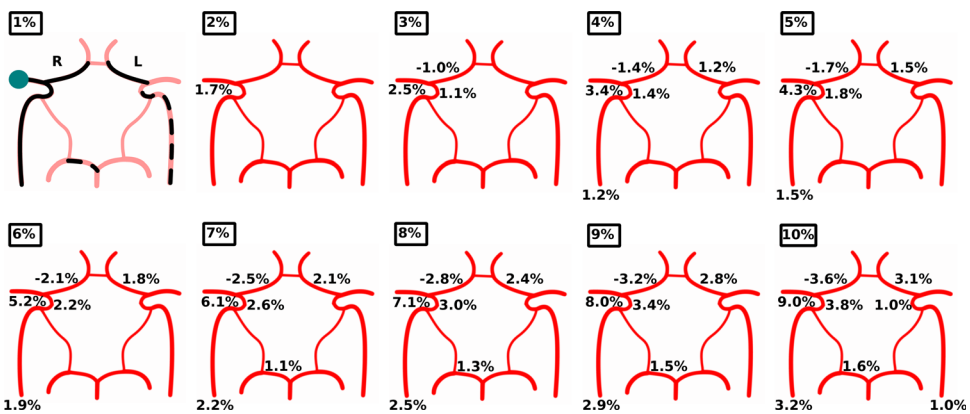

Fig. 6 Percentages of flow increase are shown at each decrease of the peripheral resistance values, indicated by the percentage in the boxes. Since a 1% did not yield notable flow, the schematic was used to denote the vessel with the decreasing R_2, highlighted by the circle, and collateral pathways. R—right, L—left, solid line—vessels that express notable flow change with a R_2 decrease of up to 5%, rounded dashed line up to a 10% decrease.

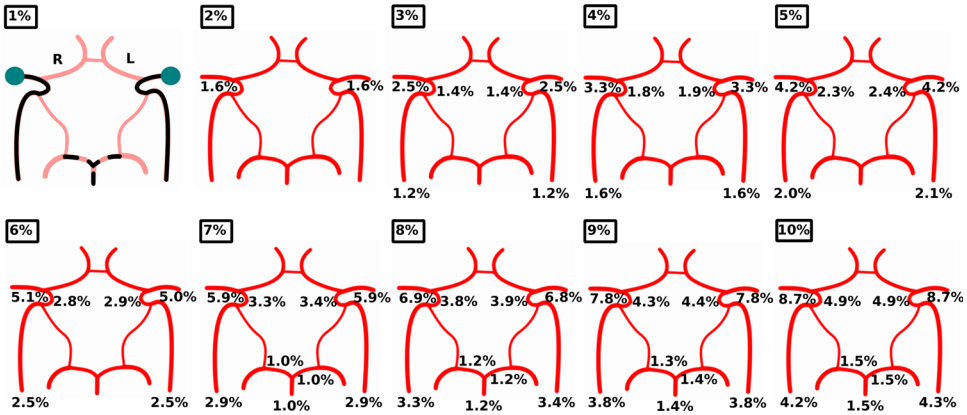

Fig. 7 Percentages of flow increase are shown at each decrease of the peripheral resistance values, indicated by the percentage in the boxes. Since a 1% did not yield notable flow, the schematic was used to denote the vessels with the decreasing R_2, highlighted by the circles, and collateral pathways. R—right, L—left, solid line—vessels that express notable flow change with a R_2 decrease of up to 5%, rounded dashed line up to a 10% decrease.

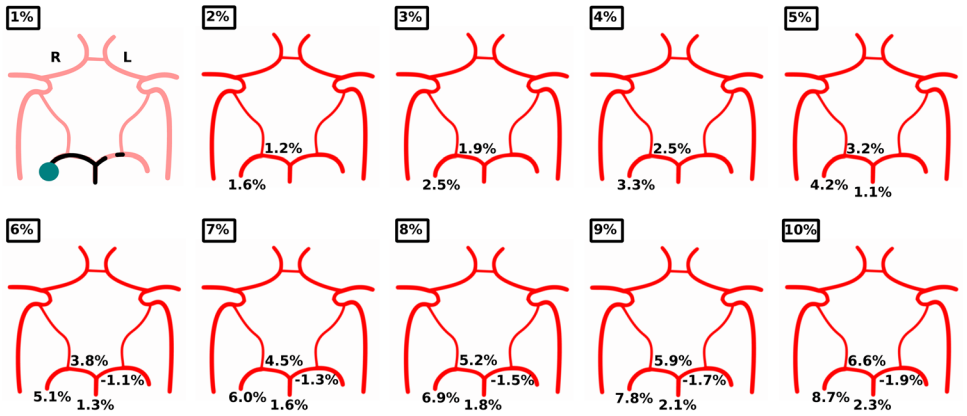

Fig. 8 Percentages of flow increase are shown at each decrease of the peripheral resistance values, indicated by the percentage in the boxes. Since a 1% did not yield notable flow, the schematic was used to denote the vessel with the decreasing R_2, highlighted by the circle, and collateral pathways. R—right, L—left, solid line—vessels that express notable flow change with a R_2 decrease of up to 5%, rounded dashed line up to a 10% decrease.

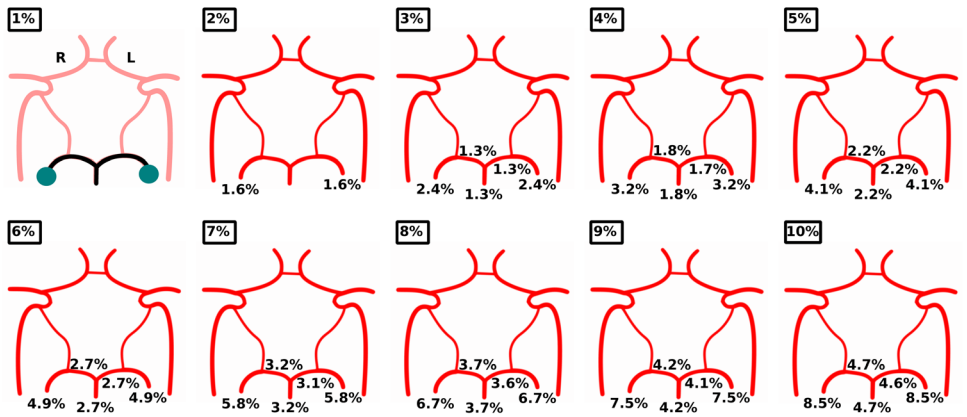

Fig. 9 Percentages of flow increase are shown at each decrease of the peripheral resistance values, indicated by the percentage in the boxes. Since a 1% did not yield notable flow, the schematic was used to denote the vessels with the decreasing R_2, highlighted by the circles, and collateral pathways. R—right, L—left, solid line—vessels that express notable flow change with a R_2 decrease of up to 5%.

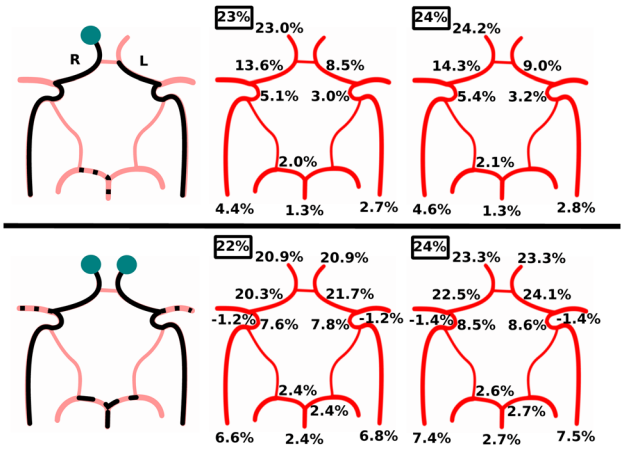

Fig. 10 Top shows the unilateral results and bottom shows the bilateral. The far left was used to denote the stimulated vessel, indicated by the circles, and collateral pathways. The middle indicates results from the SFTs: 0.27 cm^3/s increase unilaterally and 0.49 cm^3/s increase bilaterally. The right indicates the results from the MFTs: 0.28 cm^3/s unilaterally and 0.54 cm^3/s bilaterally. Percentages of R_2 decrease are located in the boxes. R–right, L–left, solid line—vessels that express notable flow change with an R_2 decrease of up to 5%, rounded dashed line up to a 10% decrease, squared dashed line decrease greater than 10%.

than a reduction of both ACAs. This is attributed to the differences in both vessel size and perfusion territory.

The ICA IIs had notable changes in flow with a unilateral R_2 decrease in the ACAs but were more affected with a bilateral reduction. These connecting vessels were highly important collateral pathways when a resistance decrease was induced in the ipsilateral MCA. The right ACA A1 and ICA II were of similar importance for supplying blood to the MCA on the same side when the reduction was unilateral. However, when a bilateral decrease was induced, the ICA IIs became the primary collateral pathway as they directly feed from the ICAs, the main afferent arteries of the CAC. The flow through the two ICA IIs was not as heavily correlated to each other as the ACA A1 segments. This was expected as the short ACoA is the only "bridge" between the two anterior vessels while the ICA IIs are separated by the ACA A1s and ACoA anteriorly and the PCoAs and PCA P1s posteriorly.

Flow in the PCoAs was considered positive if it went from the ICA to the ipsilateral PCA P1. Reversal flow through the right PCoA was induced with a unilateral R_2 reduction in the MCA. With a decrease of 10%, the change in flow went from 0.007 cm^3/s toward the PCA P1 to 0.010 cm^3/s toward the ICA. This was similar for the bilateral MCA simulations. Reductions in the PCAs did not induce any notable flow changes in the PCoAs.

The PCA P1s, as well as the BA, were important in maintaining adequate flow when the resistance was decreased in the posterior portion of the CAC. However, how they were recruited depended on if the reduction was unilaterally or bilaterally induced. Unilateral reduction of the PCAs trigged a quick compensation response in the ipsilateral PCA P1, with a reduction of only 2%. When the R_2 was decreased beyond 5%, flow began to decrease in the contralateral PCA P1. At a decrease of 10%, the flow in the ipsilateral PCA P1 increased by 0.059 cm^3/s, 0.041 cm^3/s in the BA, and 0.019 cm^3/s in the corresponding PCoA. The contralateral PCA P1 decreased by 0.017 cm^3/s and the corresponding PCoA changed from a reversal flow of 0.013 cm^3/s toward the ICA, to −0.001 cm^3/s, toward the PCA P1.

With maximum reduction in both of the PCAs, flow through the BA increased by 0.082 cm^3/s, 0.042 cm^3/s in the right PCA P1, 0.041 cm^3/s in the left PCA P1, 0.033 cm^3/s in the right PCoA, and 0.020 cm^3/s, from −0.013 cm^3/s, in the left PCoA. There was no notable affects in the other vessels with a posterior reduction of 10% in either the unilateral or bilateral test.

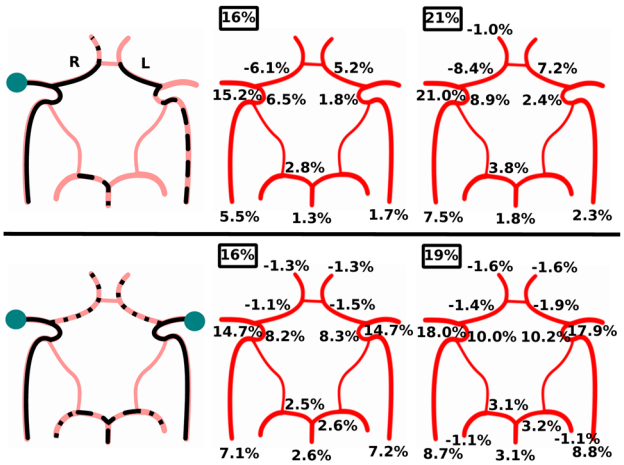

Fig. 11 Top shows the unilateral results and bottom shows the bilateral. The far left was used to denote the stimulated vessel, indicated by the circles, and collateral pathways. The middle indicates results from the SFTs: 0.27 cm^3/s increase unilaterally and 0.49 cm^3/s increase bilaterally. The right indicates the results from the MFTs: 0.36 cm^3/s unilaterally and 0.62 cm^3/s bilaterally. Percentages of R_2 decrease are located in the boxes. R—right, L—left, solid line—vessels that express notable flow change with an R_2 decrease of up to 5%, rounded dashed line up to a 10% decrease, squared dashed line decrease greater than 10%.

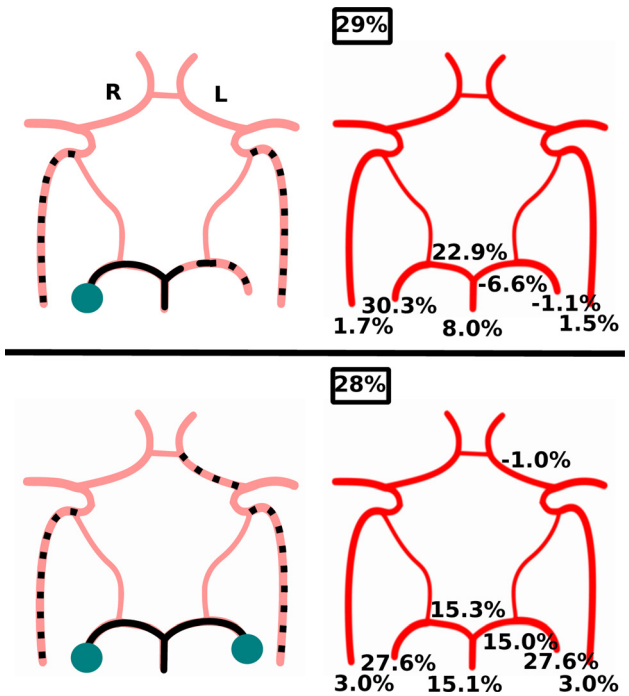

Fig. 12 Top shows the unilateral results and bottom shows the bilateral. The left was used to denote the stimulated vessel, indicated by the circles, and collateral pathways. The right indicates the results for the MFT, as this was used as the baseline for the SFT in the ACAs and MCAs reductions, 0.27 cm^3/s unilaterally and 0.49 cm^3/s bilaterally. Percentages of R_2 decrease are located in the boxes. R—right, L—left, solid line—vessels that express notable flow change with an R_2 decrease of up to 5%, rounded dashed line up to a 10% decrease, squared dashed line decrease greater than 10%.

Table 3 The value of flow (cm^3/s) decrease in the brachial and external carotid (ECA) arteries outside of the CAC in response to the different reduction tests. R—right, L—left, *—increase in flow.

Affected vessels outside of the CAC							
		Brachial		ECA		Subclavian	
Artery	R_2	R	L	R	L	R	L
Unilateral, SFT							
ACA	23%	0.012	0.013	0.008	0.007	0.001	0.001
MCA	16%	0.013	0.013	0.008	0.006	0.001	0.002
PCA	29%	0.013	0.013	0.007	0.006	0.058*	0.058*
Bilateral, SFT							
ACAs	22%	0.024	0.024	0.014	0.014	0.002	0.002
MCAs	16%	0.025	0.025	0.015	0.015	0.003	0.003
PCAs	28%	0.025	0.025	0.012	0.012	0.11*	0.11*
Unilateral, MFT							
ACA	24%	0.013	0.013	0.008	0.007	0.001	0.002
MCA	21%	0.018	0.018	0.011	0.009	0.002	0.002
PCA	29%	0.013	0.013	0.007	0.006	0.058*	0.058*
Bilateral, MFT							
ACAs	24%	0.026	0.026	0.015	0.015	0.003	0.003
MCAs	19%	0.031	0.031	0.018	0.018	0.003	0.003
PCAs	28%	0.025	0.025	0.012	0.012	0.11*	0.11*

It was maintained that if the communicating arteries were more than 1 magnitude smaller than the nearest efferent artery, changes in flow were not considered notable. This was based on the literature which argues that under normal circumstances or configurations of the CAC, flow through the communicating arteries can be considered negligible [28–34]. In a CAC that possessed a "normal" configuration, a bilateral reduction of 10% in the efferent arteries did not create a notable change in any of the communicating arteries but they contributed to the maintenance of homeostasis. Therefore, it would be more accurate to say that the communicating arteries are important in circles with "normal" configurations to compensate for the increase in metabolic demands to stimulation in different regions of the brain.

Out of the first 60 simulations, the right ICA II was the most utilized collateral pathway with a rate of 28 occurrences of notable flow change (46.7%). This was followed closely by the right ICA at 26 (43.3%) and the right PCA P1 and ACA A1 segments, both with 25 (41.7%). Note that half of the simulations were unilateral reductions; hence, the vessels were more often used as collateral pathways occurred on the right side of the circle.

When the peripheral resistance was reduced unilaterally, the main collateral pathways used were those occurring on the ipsilateral side and those that lay within the anterior portion of the circle. In contrast, bilateral reductions demanded more blood to be introduced into the system versus shunting around the circle. The afferent artery closest to the bilateral reduction exhibited notable flow change as well as the proximal connecting vessels, such as the ICA IIs as the flow from the ICAs passed through these, similar with the PCA P1s in relationship with the BA.

4.2 Same and MFTs. For the SFT in the right ACA, to obtain the desired increase of 0.27 cm^3/s as mentioned earlier, a decrease of 23% was induced in the resistance. To compensate for the demands, the CAC recruited two more vessels than those utilized at a 10% decrease, the right PCA P1 and BA. At the highest R_2 decrease, MFT at 24%, no more vessels were recruited. The same collateral pathways were used to allow for the SFT within the right MCA, at a 16% R_2 decrease, as compared with a 10% decrease. However, in the MCA MFT with a reduction of 21%, notable blood flow was drawn from the right ACA. The unilateral SFT in the PCA was also the same as the R_2 required for the MFT, 29%. For the circle to maintain homeostasis, both ICAs had notable increase in flow and the left PCA had notable decrease.

A flow increase in both ACAs, totaling 0.49 cm^3/s for the bilateral SFT, was accomplished at a 22% R_2 decrease. Five more vessels exhibited notable flow change to compensate for the demand than those required with a 10% reduction. The BA contributed more flow to the CAC, because of this, both PCA P1s displayed notable flow increases as well. Flow was also being drawn from both MCAs to supply the demand (Fig. 10). No more vessels were utilized for the MFT.

In a complete circle with a unilateral MCA stimulation, the desired amount of flow increase was obtained at an R_2 decrease of 16%. One more vessel was acquired beyond that of a 10% decrease, the BA. Almost all of the collateral pathways were utilized to compensate for the demand, only the contralateral PCA P1 was not.

To achieve the bilateral SFT increase of 0.49 cm^3/s in the MCAs, a 16% reduction in the R_2 was induced. To compensate for the demand, four more vessels were recruited: both ACAs and ACA A1 segments (Fig. 11). For the MFT, blood flow was being drawn from both PCAs. This means an R_2 decrease of 19% in both MCAs caused the most impact on the system with notable flow change in all the main vessels that compose, feed into, and leave the CAC.

The bilateral SFT or MFT, as they are the same for the PCAs, test did not have as big of an impact on the circle as only the ICAs were recruited beyond the 10% R_2 decrease, again with 28% being the maximum R_2 reduction (Fig. 12). Even with the same amount of flow increase in each efferent artery both unilaterally and bilaterally, the MCAs had the biggest impact on the system.

The vessels that compose the CAC are not the only ones that are affected by the reduced R_2 values. This is indicated by the increase flow in the vertebral and ICAs as blood supplied to these also need to be increased to compensate for the demand. Table 3 shows changes in the amount of flow through the brachials, external carotids, and subclavians. The brachials and external carotid arteries displayed decreases in flow. Conversely, there was an increase in blood flow through the subclavians with PCA reductions, as the vertebrals—which supply the posterior portion of the circle—bifurcate from them. It has been documented that the subclavians can recruit blood from the CAC, termed subclavian steal syndrome [35]. Since blood can be "stolen" from by the subclavians, it can be argued that the opposite is possible, the CAC can recruit from the subclavians as well as other arteries.

5 Conclusion

Flow through cerebral vessels depends mainly upon compliance, which does not change dramatically over a short period of time, and resistance, which is highly correlated with the vessel

radius and can change over a short period of time. The R_2 was decreased up to 10% in the efferent arteries, both unilaterally and bilaterally. Even with a bilateral reduction of the R_2 up to 10% in the largest pair of efferent arteries, there was no notable flow change within the remaining two pairs, showing that a complete CAC utilizes the collateral pathways, particularly the communicating arteries, during regional stimulation of the brain without the presence of a stenosed or occluded artery. More importantly, it shows the ability of the circle to recruit blood to supply the increase in demand without depleting blood flow from the other areas of the brain.

Upon further research, it became apparent that flow could increase beyond the scope of a 10% reduction and still be physiologically correct. Since most studies focus on velocity changes due to stimulation, the current model was used to achieve the same velocity percent changes by decreasing the peripheral resistance. These values were then used to determine the coterminous flow and observe how the CAC compensated for the increase in demand. For the SFTs, both unilaterally at 0.27 cm^3/s and bilaterally at 0.49 cm^3/s, the MCAs had the most impact on the collateral pathways of the CAC. The MCAs also had the ability to handle the largest amount of local flow increase for the MFTs, 0.36 cm^3/s unilaterally and 0.62 cm^3/s bilaterally.

There were some limitations to the present study:

(1) The configuration of the CAC was highly idealized as it was a symmetrical and complete circle.
(2) There were only the main vessels that propagate from the heart to the CAC that were included. For one to study wave progression through the body, it is better to have more vessels as the wave is partially reflected at each bifurcation. Which these reflections combine with the incoming and give the distinctive dicrotic notch to the wave profile.
(3) At the end of each truncated vessel were constant parameters, there was no autoregulatory mechanism.
(4) The reduction was only induced in the efferent pairs where it is common to have multiple regions of the brain stimulated simultaneously.

To address these limitations, circles with common variations are being tested, a missing ACA A1 segment as well as a circle with a missing PCA P1 segment. A model is also being constructed that will utilize the largest 55 arterial segments in combination with the CAC.

The current research is part of a team effort to map the processes of the brain. Focus has been on neurovascular coupling and bettering the understanding of ionic interactions within these units. Another aspect is a bifurcating H-tree that has fractal properties and is space-filling. When the models are combined, the 1D model will calculate the property changes within the systemic and cerebral arteries: flow, pressure, and velocity for example. These parameters will be communicated to the H-tree that will bifurcate for a specified number of levels with a neurovascular unit coupled to the end which represents 0.2 mm^3 of brain tissue. Individual neurovascular units will be stimulated with the ability of simulating several different physiological conditions that will affect the local blood supply. Consequently, the H-tree will relay the changes to the 1D model that will react accordingly and the cycle will continue for a given amount of time. Thus, this will be the most complete simulation of arterial flow through the body coupled with metabolic processes of the brain and autoregulation. However, before coupling the models it is essential to study the collateral patterns of a CAC without the H-tree and neurovascular units as this has never been done before to the best of the current authors' knowledge and a baseline of data is needed to allow for comparisons once coupled.

Nomenclature

ACA = anterior cerebral artery
ACA A1 = proximal segment of the anterior cerebral artery
ACoA = anterior communicating artery
BA = basilar artery
CAC = cerebral arterial circle
ICA = internal carotid artery
ICA II = segment of the internal carotid artery that lays within the cerebral arterial circle
MCA = middle cerebral artery
MFT = maximum flow test
PCA = posterior cerebral artery
PCA P1 = proximal segment of the posterior cerebral artery
PCoA = posterior communicating artery
R_2 = peripheral resistance
SFT = same flow test

References

[1] Moritz, A., Koci, G., Steinlechner, B., Hölzenbein, T., Nasel, C., Grubhofer, G., and Dworschak, M., 2007, "Contralateral Stroke During Carotid Endarterectomy Due to Abnormalities in the Circle of Willis," Middle Eur. J. Med., **119**(21–22), pp. 669–673.
[2] Dormanns, K., van Disseldorp, E., Brown, R., and David, T., 2015, "Neurovascular Coupling and the Influence of Luminal Agonists Via the Endothelium," J. Theor. Biol., **364**, pp. 49–70.
[3] Farr, H., 2012, "Autoregulation of the Human Cerebrovasculature by Neurovascular Coupling or a Collection of Stories About Mathematics and the Mind," Ph.D. thesis, University of Canterbury, Christchurch, NZ.
[4] Filosa, J. A., Bonev, A. D., and Nelson, M. T., 2004, "Calcium Dynamics in Cortical Astrocytes and Arterioles During Neurovascular Coupling," Circ. Res., **95**(10), pp. e73–e81.
[5] Iadecola, C., 2004, "Neurovascular Regulation in the Normal Brain and in Alzheimer's Disease," Nat. Rev. Neurosci., **5**(5), pp. 347–360.
[6] Willie, C. K., Cowan, E. C., Ainslie, P. N., Taylor, C. E., Smith, K. J., Sin, P. Y. W., and Tzeng, Y. C., 2011, "Neurovascular Coupling and Distribution of Cerebral Blood Flow During Exercise," J. Neurosci. Methods, **198**(2), pp. 270–273.
[7] Thakker, B., and Vyas, A. L., 2011, "Pulse Classifier for Suppressed Dicrotic Notch Pulse," Int. J. Mach. Comput., **1**(2), pp. 148–153.
[8] Alastruey, J., Parker, K. H., Peiró, J., Byrd, S. M., and Sherwin, S. J., 2007, "Modeling the Circle of Willis to Assess the Effects of Anatomical Variations and Occlusions on Cerebral Flows," J. Biomech., **40**(8), pp. 1794–1805.
[9] Anzola, G. P., Gasparotti, R., Magoni, M., and Prandini, F., 1995, "Transcranial Doppler Sonography and Magnetic Resonance Angiography in the Assessment of Collateral Hemispheric Flow in Patients With Carotid Artery Disease," Stroke, **26**(2), pp. 214–217.
[10] Baumgartner, R. W., Baumgartner, I., Mattle, H. P., and Schroth, G., 1997, "Transcranial Color-Coded Duplex Sonography in the Evaluation of Collateral Flow Through the Circle of Willis," Am. J. Neuroradiol., **18**(1), pp. 127–133.
[11] Cassot, F., Vergeur, V., Bossuet, P., Hillen, B., Zagzoule, M., and Marc-Vergnes, J.-P., 1995, "Effects of Anterior Communicating Artery Diameter on Cerebral Hemodynamics in Internal Carotid Artery Disease: A Model Study," Circulation, **92**(10), pp. 3122–3131.
[12] Derdeyn, C. P., Videen, T. O., Fritsch, S. M., Carpenter, D. A., Grubb, R. L., and Powers, W. J., 1999, "Compensatory Mechanisms for Chronic Cerebral Hypoperfusion in Patients With Carotid Occlusion," Stroke, **30**(5), pp. 1019–1024.
[13] Fahy, P., Malone, F., McCarthy, E., McCarthy, P., Thornton, J., Brennan, P., O'Hare, A., Looby, S., Sultan, S., Hynes, N., and Morris, L., 2015, "An In Vitro Evaluation of Emboli Trajectories Within a Three-Dimensional Physical Model of the Circle of Willis Under Cerebral Blood Flow Conditions," Ann. Biomed. Eng., **43**(9), pp. 2265–2278.
[14] Haripriya, M., and Melani, R. S., 2010, "A Study of the Anatomical Variations of the Circle of Willis Using Magnetic Resonance Imaging," Int. J. Anat. Sci., **1**, pp. 21–25.
[15] Sherwin, S. J., Willemet, M., and Alastruey, J., 2014, *Nektar1D Reference Manual*, Department of Aeronautics, Imperial College, London.
[16] Xiao, N., Alastruey, J., and Figueroa, A. C., 2014, "A Systematic Comparison Between 1-D and 3-D Hemodynamics in Compliant Arterial Models," Int. J. Numer. Methods Biomed. Eng., **30**(2), pp. 204–231.
[17] Alastruey, J., Khir, A. W., Matthys, K. S., Segers, P., Sherwin, S. J., Verdonck, P. R., Parker, K. H., and Peiró, J., 2011, "Pulse Wave Propagation in a Model Human Arterial Network: Assessment of 1-D Visco-Elastic Simulations Against In Vitro Measurements," J. Biomech., **44**(12), pp. 2250–2258.
[18] Alastruey, J., Parker, K. H., Peir, J., and Sherwin, S. J., 2009, "Analysing the Pattern of Pulse Waves in Arterial Networks: A Time-Domain Study," J. Eng. Math., **64**(4), pp. 331–351.
[19] Sherwin, S. J., Formaggia, L., Peiro, J., and Franke, V., 2003, "Computational Modelling of 1D Blood Flow With Variable Mechanical Properties and Its Application to the Simulation of Wave Propagation in the Human Arterial System," Int. J. Numer. Methods Fluids, **43**(6–7), pp. 673–700.
[20] Stergiopulos, N., Young, D. F., and Rogge, T. R., 1992, "Computer Simulation of Arterial Flow With Applications to Arterial and Aortic Stenoses," J. Biomech., **25**(12), pp. 1477–1488.

[21] Fahrig, R., Nikolov, H., Fox, A. J., and Holdsworth, D. W., 1999, "A Three-Dimensional Cerebrovascular Flow Phantom," Med. Phys., **26**(8), pp. 1589–1599.
[22] Moore, S. M., Moorhead, K. T., Chase, J. G., David, T., and Fink, J., 2005, "One-Dimensional and Three-Dimensional Models of Cerebrovascular Flow," ASME J. Biomech. Eng., **127**(3), pp. 440–449.
[23] Kelley, R. E., Chang, J. Y., Scheinman, N. J., Levin, B. E., Duncan, R. C., and Lee, S. C., 1992, "Transcranial Doppler Assessment of Cerebral Flow Velocity During Cognitive Tasks," Stroke, **23**(1), pp. 9–14.
[24] Linkis, P., Jorgensen, L. G., Olesen, H. L., Madsen, P. L., Lassen, N. A., and Secher, N. H., 1994, "Dynamic Exercise Enhances Regional Cerebral Artery Mean Flow Velocity," J. Appl. Physiol., **78**(1), pp. 12–16.
[25] Madsen, P. L., Sperling, B. K., Warming, T., Schmidt, J. F., Secher, N. H., Wildschiødtz, G., Holm, S., and Lassen, N. A., 1993, "Middle Cerebral Artery Blood Velocity and Cerebral Blood Flow and O_2 Uptake During Dynamic Exercise," J. Appl. Physiol., **74**(1), pp. 245–250.
[26] Spelsberg, B., Bohning, A., Kompf, D., and Kessler, C., 1998, "Visually Induced Reactivity in Posterior Cerebral Artery Blood Flow," J. Neuro-Ophthalmol., **18**(4), pp. 263–267.
[27] Urban, P. P., Allardt, A., Tettenborn, B., Hopf, H. C., Pfennigsdorf, S., and Lieb, W., 1995, "Photoreactive Flow Changes in the Posterior Cerebral Artery in Control Subjects and Patients With Occipital Lobe Infarction," Stroke, **26**(10), pp. 1817–1819.
[28] Devault, K., Gremaud, P. A., Novak, V., Olufsen, M. S., Vernieres, G., and Zhao, P., 2008, "Blood Flow in the Circle of Willis: Modeling and Calibration," Multiscale Model. Simul., **7**(2), pp. 888–909.
[29] Hartkamp, M. J., van Der Grond, J., van Everdingen, K. J., Hillen, B., and Mali, W. P., 1999, "Circle of Willis Collateral Flow Investigated by Magnetic Resonance Angiography," Stroke, **30**(12), pp. 2671–2678.
[30] Hoksbergen, A. W. J., Majoie, C. B. L., Hulsmans, F.-J. H., and Legemate, D. A., 2003, "Assessment of the Collateral Function of the Circle of Willis: Three-Dimensional Time-of-Flight MR Angiography Compared With Transcranial Color-Coded Duplex Sonography," Am. J. Neuroradiol., **24**(3), pp. 456–462.
[31] Kim, C. S., 2007, "Numerical Simulation of Auto-Regulation and Collateral Circulation in the Human Brain," J. Mech. Sci. Technol., **21**(3), pp. 525–535.
[32] Sushma, R. K., D'Souza, A. S., and Bhat, K. M. R., 2014, "Fetal and Primitive Type of Circle of Willis With Unilateral Trifurcation of Internal Carotid Artery," Med. Science, **3**(3), pp. 1530–1537.
[33] Razavi, S. E., and Sahebjam, R., 2014, "Numerical Simulation of the Blood Flow Behavior in the Circle of Willis," Bioimpacts, **4**(2), pp. 89–94.
[34] Viedma, A., Jimenez-Ortiz, C., and Marco, V., 1997, "Extended Willis Circle Model to Explain Clinical Observations in Periorbital Arterial Flow," J. Biomech., **30**(3), pp. 265–272.
[35] Amini, R., Gornik, H. L., Gilbert, L., Whitelaw, S., and Shishehbor, M., 2011, "Bilateral Subclavian Steal Syndrome," Case Reports Cardiol., **2011**, p. 146267.